Article

A Low Switching Frequency Model Predictive Control Method for an Induction Motor Fed by a 3-Level Inverter

Jingtao Huang [1,*], Guangxu Jiang [1], Peng Zhang [2] and Jixin Chen [1]

[1] College of Information Engineering, Henan University of Science and Technology, Luoyang 471023, China
[2] China Railway Engineering Equipment Group Co., Ltd., Zhengzhou 450016, China
* Correspondence: jthuang@haust.edu.cn

Abstract: Traditional model predictive control (MPC) for the induction motor fed by a three-level inverter needs to explore 27 voltage vectors to obtain the optimal one, which leads to high switching frequency and requires too much computation. To solve this issue, a low switching frequency model predictive control with partition optimization is proposed. First, the reference voltage vector can be gained from the prediction model at the next time, and the space voltage vector plane is divided into 12 sectors for further vector choice. Furthermore, considering inverter constraints, the candidate voltage vectors are determined according to the sector location of the reference voltage vector. In this way, the candidate vectors can be reduced to 3 at most. Then, a boundary circle limit is designed to avoid unnecessary switch changes. If the reference voltage vector is within the boundary limit, the switches do not act, which can reduce the system switching frequency without introducing the extra weight coefficient into the cost function. These selected voltage vectors are substituted into the cost function to determine the optimal one. Finally, the neutral point voltage deviation is controlled by the positive and negative redundant small vectors to realize the multi-objective constraint without weighting coefficients. The simulation results show that the proposed control method can significantly reduce the switching frequency; at the same time, both the dynamic and steady performances can be maintained well, and the cost function has no weight coefficients.

Keywords: induction motor; three-level inverter; model predictive control; weighting coefficients; partition optimization; low switching frequency

1. Introduction

The induction motor (IM) has been widely used in electric drive systems due to the advantages of easy maintenance and high reliability [1–4]. Vector control (VC) and direct torque control (DTC) are currently the most widely used high-performance control methods in the industry [5–8]. VC has good dynamic performance, but the system response is slow. DTC can improve the system response speed but tends to cause flux waveform distortion and large torque ripple [9]. To solve the shortcomings of VC and DTC, model predictive control (MPC) has attracted considerable attention to improving the performance of motor control systems [10–13].

MPC has the advantages of a simple and intuitive concept, good control performance, easy to deal with nonlinear constraints, etc. For motor control, it is known as model predictive torque control (MPTC) or model predictive current control (MPCC) [14–17]. Among them, MPTC has the advantage of high real-time response, but traditional MPTC considers both torque and flux variables at the same time, so it needs to add a weight coefficient into the cost function to balance the effect of flux and torque. However, until now, there is no mature method to decide the weight coefficient, so it is difficult to obtain the optimal weight coefficient [18,19].

Compared to traditional two-level inverters, 3-level neutral-point clamped (3L-NPC) inverters have the advantages of low output harmonic components, low voltage distortion,

and lower voltage stress, so they are widely used [20–23]. However, the 3L-NPC inverter has 27 voltage vectors, and traditional MPTC needs to enumerate all the voltage vectors in the cost function to obtain the optimal solution, which greatly increases the calculation cost and reduces the real-time performance of the control system. In [24], the set of candidate voltage vectors is selected in four cases according to the torque variation and the flux variation, but the switching restriction is not taken into account and results in uneven output voltage and high harmonics. In [25], the number of candidate voltages is reduced to 15 by eliminating the inverter switching states that violate the principle of voltage level change, but the calculation amount also remains large. In [26], the authors constructed a vector preselection table that forbids the voltage level from changing from high to low directly, but it is still necessary to explore 12 voltage vectors. In [27], passivity-based control is used to calculate the cross-section of the optimal voltage vector and prove its stability; the voltage vectors in the cross-section are reduced to 8. In [28], the authors proposed a sector-based control algorithm, which reduces the number of candidate voltage vectors to 7. In [29], by building inverter constraints, the authors reduced the number of calculation voltage vectors to 5~13, but it would be better to continue reducing the number of calculation voltage vectors. Reducing the candidate voltage vectors has become a central issue in MPC implementation for 3-level inverter control. If the number of candidate vectors can be further reduced, it will be conducive to improving the real-time performance of the system and reducing the switching frequency.

In this work, a model predictive vector control method with boundary circle limit partition optimization (BLMPVC) is proposed to reduce the switching frequency. Firstly, the predictive model of an IM is constructed to calculate the reference voltage vector at the next moment, and a sector partition optimization control method is proposed to divide the basic voltage vector space into 12 sectors, and the candidate voltage vectors are selected according to the inverter switch change limit and the sector where the reference voltage vector located, so that the candidate vectors can be reduced to 1~3. Furthermore, a boundary circle limit is designed to reduce the switching frequency of the system, and the cost function does not have an additional constraint term. Then, the neutral point voltage is balanced by using positive and negative redundant small vectors. In this way, the multi-objective constraint control can be realized without weight coefficients. Finally, the simulations were carried out to verify the proposed method. The BLMPVC control strategy proposed in this paper has the following features:

(1) Based on vector partitioning, the number of candidate voltage vectors can be reduced from 27 to 1~3, and the computation cost of the control system is significantly reduced without affecting the responses.
(2) The switching frequency is greatly reduced without performance deteriorating, which is achieved by the boundary circle limiting strategy.
(3) The cost function can realize multi-objective constraints without weight coefficients and avoid tedious weight factor tuning, which is user-friendly.

The structure of this paper is as follows. Section 2 discusses the mathematical model of the induction motor, Section 3 discusses the traditional MPVC control principle, Section 4 presents the improved BLMPVC control method, Section 5 gives the simulation results, and Section 6 concludes the work.

2. Model of the Induction Motor

The stator current i_s and stator flux ψ_s are the state variables in the two-phase static coordinate system. The mathematical model of an induction motor can be expressed as follows,

$$\left.\begin{array}{c} \frac{\mathrm{d}x}{\mathrm{d}t} = Ax + Bu \\ y = Cx \end{array}\right\} \tag{1}$$

where,

$$A = \begin{bmatrix} -\lambda(R_s L_r + R_R L_S) + j\omega_r & \lambda(R_r - jL_r\omega_r) \\ -R_s & 0 \end{bmatrix}$$

$$B = \begin{bmatrix} \lambda L_r \\ 1 \end{bmatrix}, C = \begin{bmatrix} 1 & 0 \end{bmatrix}, x = \begin{bmatrix} i_s \\ \psi_s \end{bmatrix}$$

R_s and R_r are the stator and rotor resistances of the motor; L_s, L_r, L_m are stator inductance, rotor inductance, and mutual inductance; ω_r is the electrical rotor speed; u is the stator voltage; i_s is the stator current; ψ_s is the stator flux; $\lambda = 1/(L_sL_r - L_m^2)$.

The Heun method [30] is used to discretize the mathematical model of the IM. The mathematical model after discretization is as follows,

$$\left. \begin{array}{l} x_p(k+1) = x(k) + T_{sc}[Ax(k) + Bu(k)] \\ x(k+1) = x_p(k+1) + \frac{T_{sc}}{2}A[x_p(k+1) - x(k)] \end{array} \right\} \tag{2}$$

where T_{sc} is the control period; $x(k)$ is the state variable of the present moment; $x_p(k+1)$ is the prediction correction variable; $x(k+1)$ is the predicted state variable at the next time. The rotor flux at the next time ψ_r^{k+1} can be obtained by the stator flux at the next time ψ_s^{k+1} and the stator current i_s^{k+1} as follows,

$$\psi_r^{k+1} = \frac{L_r}{L_m}\psi_s^{k+1} - \frac{1}{\lambda L_m}i_s^{k+1} \tag{3}$$

The electromagnetic torque at the next time is:

$$T_e^{k+1} = \frac{3}{2}N_p\lambda L_m\left(\psi_s^{k+1} \otimes \psi_s^{k+1}\right) \tag{4}$$

where N_p represents the pole number of the induction motor.

3. Traditional MPVC Control

3.1. MPVC Scheme

Figure 1 shows the MPVC scheme for the induction motor fed by a 3L-NPC inverter. First, the stator current i_s^k, stator voltage u_s^k, and rotor speed ω_r^k were gained by measurement or calculation, and the stator flux ψ_s^k was observed by the full-order flux observer. The torque reference value T_e^{ref} was obtained by the PI controller from the deviation between the given speed ω_r^{ref} and ω_r^k. The stator current i_s^{k+1}, stator flux ψ_s^{k+1}, and rotor flux ψ_r^{k+1} at the next moment were predicted by the motor model (full order observer). The stator flux amplitude ψ^{ref} is set to the stator flux amplitude of the motor at rated work conditions. Then the reference voltage vector u_s^{ref} at the next moment, is calculated according to the principle of the deadbeat control of flux torque. Substitute the u_s^{ref} for the next time into the cost function to find the optimal voltage vector for the next time. The inverter outputs the optimal voltage vector to complete the control.
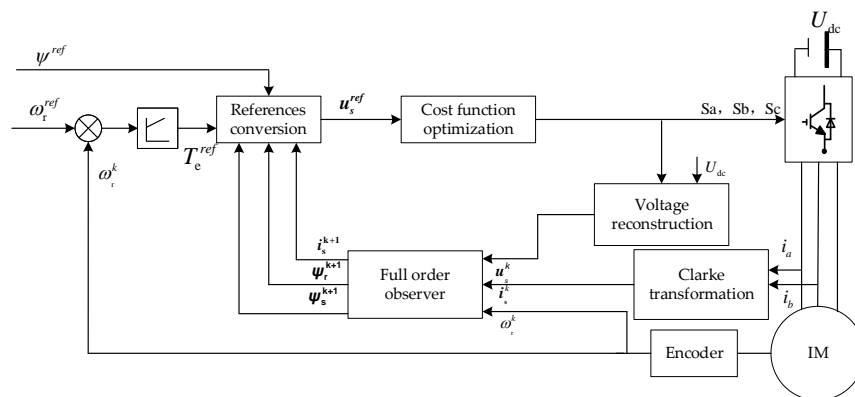

Figure 1. Diagram of MPVC.

The flow chart of MPVC is shown in Figure 2. The control procedure is implemented at a constant period. In every control period, the actual voltage, current, and speed are obtained and fed back to the prediction model to obtain the predicted system status, i.e., i_s^{k+1}, ψ_s^{k+1}, and ψ_r^{k+1}. Then calculate u_s^{ref} with the system status prediction and the required values of T_e^{ref} and ψ^{ref}. By exploring the candidate vectors, the optimal one with respect to the cost function can be found. Additionally, the optimal voltage vector is carried on the inverter to change the output AC power, then the motor can be controlled. If the system is not shut down or interrupted, this control cycle repeats at a constant period.
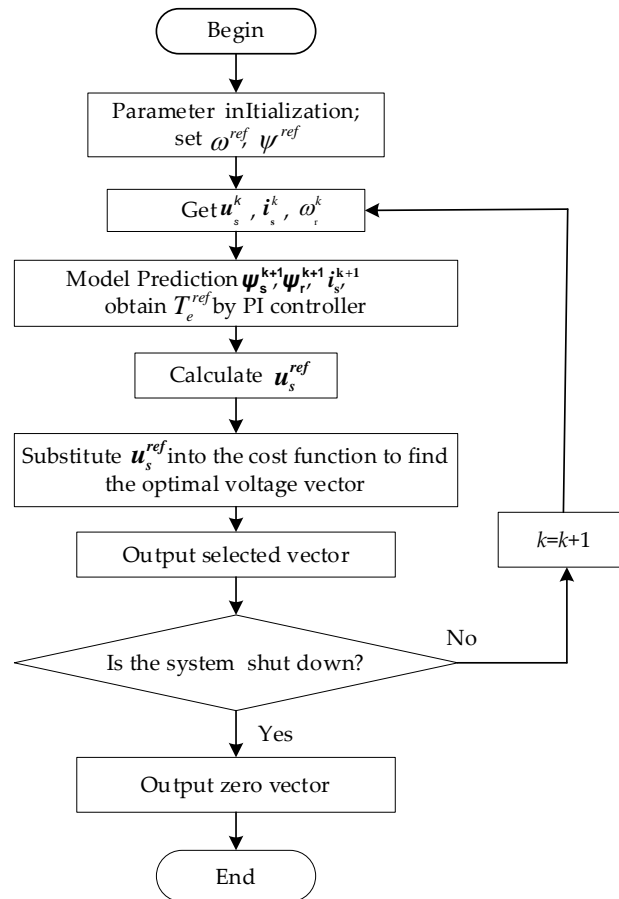

Figure 2. Flow chart of MPVC.

3.2. Predictive Flux Control Model

According to the deadbeat control, the torque reference value T_e^{ref} and stator flux amplitude reference value ψ^{ref} were substituted for the next moment. That is,

$$\left|\psi_s^{k+1}\right| = \psi^{ref} \tag{5}$$

$$T_e^{k+1} = T_e^{ref} \tag{6}$$

To make the electromagnetic torque approach its reference value in the next control cycle, the slip angle $\angle\theta_{sr}$ at the next moment can be calculated as follows,

$$\angle\theta_{sr} = arcsin\left(T_e^{ref} / \frac{3}{2}N_p\lambda L_m\left|\psi_r^{k+1}\right|\psi^{ref}\right) \tag{7}$$

where ψ_r^{k+1} can be obtained by Equation (3).

The new stator flux vector reference value ψ_s^{ref} angle is

$$\angle \psi_s^{ref} = \angle \psi_r^{k+1} + \angle \theta_{sr} \tag{8}$$

Combined with Equations (5) and (8), the new reference value of the stator flux vector is

$$\boldsymbol{\psi}_s^{ref} = \psi^{ref} \cdot \exp\left(j \bullet \angle \psi_s^{ref}\right) \tag{9}$$

With the new stator flux vector reference value $\boldsymbol{\psi}_s^{ref}$, the stator voltage vector reference value can be calculated by Equation (10) according to the deadbeat control.

$$\boldsymbol{u}_s^{ref} = R_s \boldsymbol{i}_s^{k+1} + \frac{\boldsymbol{\psi}_s^{ref} - \boldsymbol{\psi}_s^{k+1}}{T_{SC}} \tag{10}$$

So, the control of torque and stator flux is equivalent to the control of the stator voltage vector. Thus, it can eliminate the weight coefficient of the traditional MPTC flux and torque control.

3.3. Prediction of Neutral Point Voltage Deviation

The topology of the 3L-NPC inverter is shown in Figure 3. Compared to the two-level inverter, the 3L-NPC inverter can output medium and small vectors, but it also faces the problem of the neutral point voltage deviation caused by the inflow and outflow of the neutral point current i_{np} on the DC link capacitor. The expression of the neutral point current i_{np} of the 3L-NPC inverter is:

$$i_{np} = \sum_{x=a,\,b,\,c} (1-|S_x - 1|)\, i_x \tag{11}$$

where S_x is the switching state of the inverter. Under different switching states, each part can be connected to the positive (P), neutral (O), or negative (N) on the DC link. In this work, "2" represents "P", "1" represents "O", and "0" represents "N". When $S_x = 2$ or 0, the neutral point current i_{np} is 0. When $S_x = 1$, the neutral point current i_{np} is related to the present three-phase current values.
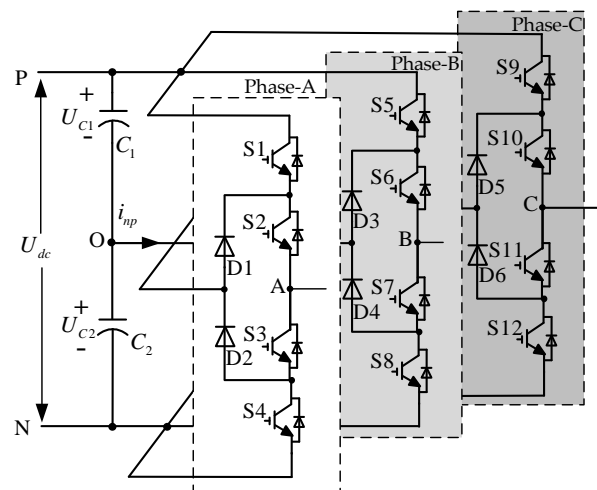

Figure 3. 3L-NPC inverter topology.

The neutral point voltage deviation U_o is defined as:

$$U_o = \frac{U_{c1} - U_{c2}}{2} \tag{12}$$

where U_{c1} and U_{c2}, respectively, represent the voltage of DC capacitors C_1 and C_2 and meet $\mathrm{d}U_{c1}/\mathrm{d}t = i_{c1}/C_1$, $\mathrm{d}U_{c2}/\mathrm{d}t = i_{c2}/C_2$, $C_1 = C_2 = C$. In summary,

$$\frac{\mathrm{d}U_o}{\mathrm{d}t} = -\frac{1}{2C} \sum_{x=a,b,c} (1-|S_x-1|)\, i_x \tag{13}$$

After the discretization of Equation (13), the neutral point voltage deviation at the next moment is:

$$U_o^{k+1} = U_o^k + \frac{T_s}{2C} \sum_{x=a,b,c} (1-|S_x-1|)\, i_x \tag{14}$$

3.4. Cost Function

Cost function plays a key role in MPC, which directs the optimization process. $n_{sw} = \sum_{x=\{a,\,b,\,c\}} \left| S_x^{k+1} - S_x^k \right|$ is the number of switch transitions between the switch states in the next time and that in the last control period. To reduce the switching numbers of the system, the cost function can be expressed as:

$$J = \left| u_s^{ref} - v^{k+1} \right| + K_{neu} \left| \Delta U_o^{k+1} \right|^2 + K_n n_{sw} \tag{15}$$

where the v^{k+1} is the inverter output voltage vector, and it is decided by the switch state $S_a^{k+1}, S_b^{k+1}, S_c^{k+1}$. K_{neu} is the weight coefficient of neutral point voltage deviation balance, K_n is the weight coefficient of switching frequency, and the size of K_{neu} and K_n can be adjusted according to needs.

4. Improved MPVC Control with Optimized Partition

4.1. Space Vector Partition Selection Method

Figure 4 shows the space voltage vector distribution of the 3L-NPC inverter. V_0 to V_{26} correspond to the basic voltage vectors 0-0-0 to 2-2-2. If all the voltage vectors are enumerated for optimization as in the traditional MPC, the calculation amount of the system will be enormously increased and the real-time control will be limited. To solve this problem, a partition optimization method is proposed. According to the inverter constraint, a phase switching state is allowed to transition at most once within adjacent control periods, that is, the switching state can only transition from 0 to 1, or from 1 to 2. It can reduce the switching frequency and avoid the problem of dynamic voltage equalization of the inverter and large harmonics on the load side. In this method, the advantages of the 3L-NPC inverter can remain. Based on this, the candidate voltage vectors can be reduced to 4~7. On this basis, the candidate vectors can be further reduced to 1~3 according to the sector where the reference voltage vector is located.

The number of candidate vectors can be reduced in the following two steps.

Step 1 Establish the inverter constraint conditions to reduce the number of candidate vectors to 4~7;

Step 2 Divide the space voltage vector plane into 12 sectors with a boundary of 30 degrees, as shown in Figure 4. Depending on the sector of the reference voltage vector and the constraints of the inverter, the vector preselection table is established as Table 1. Then the number of candidate voltage vectors can be reduced further to 1~3.

The angle between the reference voltage vector and α axis is $\theta^{ref} = \arctan\left(\dfrac{u_{s,\,\beta}^{ref}}{u_{s,\,\alpha}^{ref}} \right)$, where $u_{s,\,\alpha}^{ref}$ stands for α-axis component of u_s^{ref}, $u_{s,\,\beta}^{ref}$ stands for the β-axis component of u_s^{ref}. According to θ^{ref}, the sector where the reference voltage vector is located can be determined. When θ^{ref} is between $[0 \sim \pi/6)$, the reference voltage vector is in Sector I. Similarly, the sector where the reference voltage vector is located can be obtained.
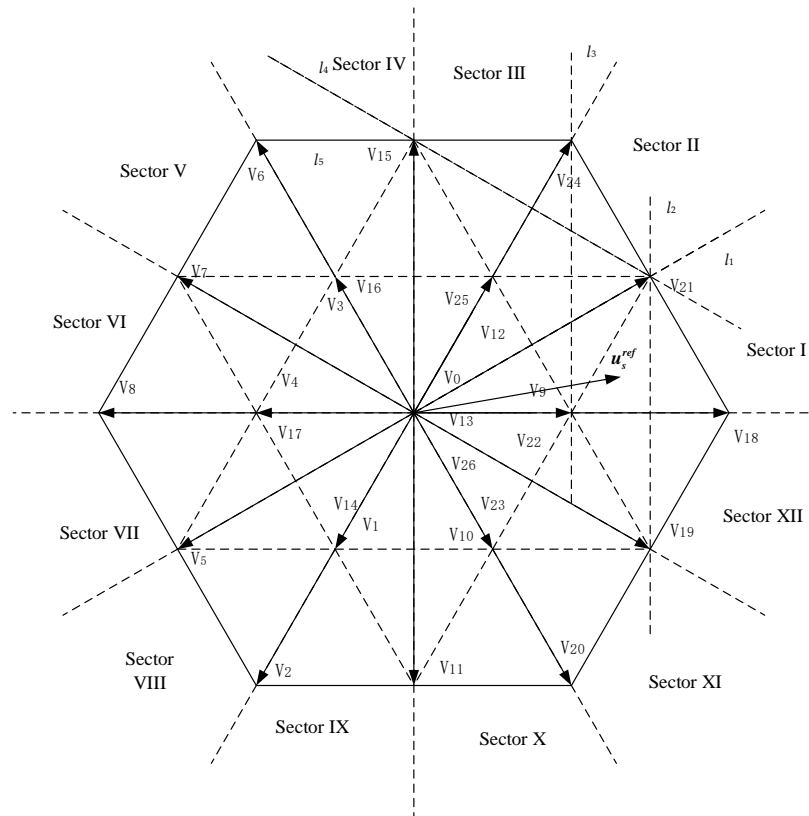
Figure 4. Distribution of the voltage vector of the 3L-NPC inverter.

Table 1. Vector preselection table.

Present Voltage Vector	Candidate Voltage Vector for Each Sector at the Next Time											
	I	**II**	**III**	**IV**	**V**	**VI**	**VII**	**VIII**	**IX**	**X**	**XI**	**XII**
V_0	V_0 V_9	V_0 V_9	V_0 V_3	V_0 V_3	V_0 V_3	V_0 V_3	V_0 V_1	V_0 V_1	V_0 V_1	V_0 V_1	V_0 V_9	V_0 V_9
V_9	V_0 V_9 V_{18}	V_0 V_{12}	V_0 V_{12}	V_0 V_{12}	V_0 V_{12}	V_0	V_0	V_0 V_{10}	V_0 V_{10}	V_0 V_{10}	V_0 V_{10}	V_0 V_9 V_{18}
V_{13}	V_{13} V_{22}	V_{12} V_{13}	V_{12} V_{13}	V_{13} V_{16}	V_{13} V_{16}	V_4 V_{13}	V_4 V_{13}	V_{13} V_{14}	V_{13} V_{14}	V_{10} V_{13}	V_{10} V_{13}	V_{13} V_{22}
V_{18}	V_9 V_{18} V_{21}	V_9 V_{21}	V_9 V_{21}	V_9 V_{21}	V_9	V_9	V_9	V_9	V_9 V_{19}	V_9 V_{19}	V_9 V_{19}	V_9 V_{18} V_{19}
V_{21}	V_{18} V_{21} V_{22}	V_{12} V_{21} V_{24}	V_{12} V_{24}	V_{12}	V_{12}	V_{12}	V_{12}	V_{22}	V_{22}	V_{22}	V_{22}	V_{18} V_{22}
V_{22}	V_{13} V_{21} V_{22}	V_{13} V_{21} V_{25}	V_{13} V_{25}	V_{13} V_{25}	V_{13} V_{25}	V_{13}	V_{13}	V_{13} V_{23}	V_{13} V_{23}	V_{13} V_{23}	V_{13} V_{19} V_{23}	V_{13} V_{19} V_{22}

As shown in Figure 4, the output voltage vector of the inverter is V_{21}. For example, according to the constraints of the inverter, the vector V_{21} allowed to arrive at the next moment is one of V_{12}, V_{18}, V_{21}, V_{22}, V_{24}. When the reference voltage vector u_s^{ref} is in Sector I, and it is below the vertical bisector l_1 of V_{18} and V_{24}. Obviously, u_s^{ref} is closer to V_{18} other than V_{24}, and it is closer to V_{22} other than V_{12}, so V_{12} and V_{24} can be excluded, and the

candidate voltage vectors can only be selected from V_{18}, V_{21}, and V_{22}. Similarly, when u_s^{ref} is in sector II, V_{18} and V_{22} can be excluded, and V_{12}, V_{21} and V_{24} are the candidate vectors. The candidate voltage vectors at the next time are determined according to the location of the u_s^{ref}. The above analysis shows that the number of candidate voltage vectors can be reduced from 27 to 1~3. In addition, the vector preselection table is constructed for the 6 typical basic vectors in sector I, as shown in Table 1. Selection of candidate vectors for other sectors can be obtained through a simple sector transformation.

4.2. Boundary Circle Limit

In the motor control system, the inverter loss is mainly the switching loss of the power switch, so the switching frequency should be maintained as low as possible. In traditional MPVC, a constraint term of the switching frequency is added to the cost function. Additionally, if you set an appropriate weight coefficient, the system may behave with a good control effect with a low switching frequency. However, the setting of the weight coefficient is complicated, and there is no good setting scheme at present. In this paper, the boundary circle restriction is introduced into MPVC, and the voltage vector selection method with the boundary circle restriction is constructed. It can help reduce the switching actions without the weight coefficient of the switching frequency in the cost function.

Figure 5 shows the optimal voltage vector selection mechanism with the boundary circle limit. First, the vertex of the output voltage vector u_v of the inverter at the present moment is taken as the circle center, then the preset maximum voltage deviation $|\Delta u_{max}|$ is taken as the radius to construct the boundary circle. Equation (10) predicts the reference voltage vector u_s^{ref} at the next moment and then judges whether u_s^{ref} is located in the boundary circle. When the error $|\Delta u|$ between u_s^{ref} and the present-voltage vector u_v is not greater than $|\Delta u_{max}|$, the voltage vector error at this time is considered to be small enough. Then the present switching state is continued to be selected without change to reduce the switching frequency. When $|\Delta u|$ is greater than $|\Delta u_{max}|$, the error is considered to be large enough, the candidate voltage vectors should be selected according to the vector preselection table, and the optimal voltage vector should be found by enumeration. The physical meaning of $|\Delta u_{max}|$ in this algorithm is the tolerance degree of the voltage control deviation, so the complicated tuning of the weight coefficient can be waived by simply and intuitively adjusting the size of $|\Delta u_{max}|$. The simulation verifies that one good option of $|\Delta u_{max}|$ is one-third of the length of the large vector, which can reduce the switching frequency and ensure the control performance.
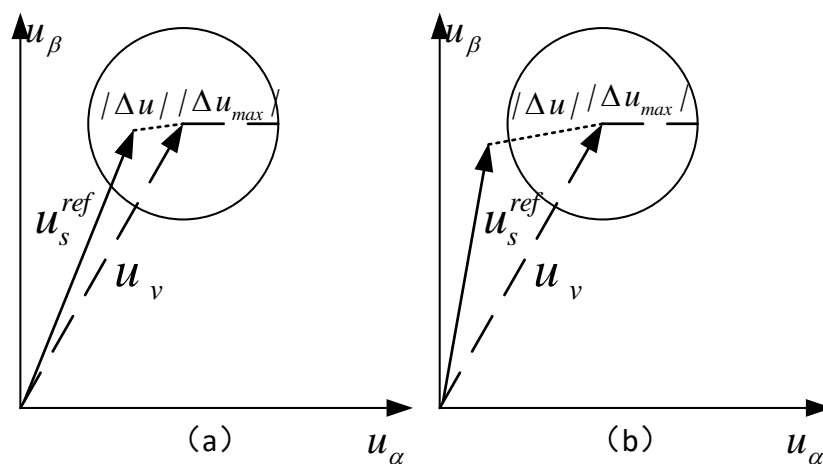

Figure 5. Boundary circle limit. (**a**) u_s^{ref} is in the boundary; (**b**) u_s^{ref} is out of the boundary.

4.3. Balancing Method of Neutral Point Voltage Deviation

From Equation (11), we can see that only the medium vector and small vector can generate a neutral point current i_{np}. So only they can charge and discharge the DC link capacitor, resulting in the change of neutral point voltage deviation U_o. The positive direction of the three-phase current i_a, i_b and i_c is defined as the direction of current flowing into the motor. When the current is positive, the influence of the medium and small vectors on the neutral point voltage deviation is shown in Table 2.

Table 2. Relationship between medium/small vector and neutral point voltage deviation.

Small Vector	U_o	Small Vector	U_o	Medium Vector	U_o
ONN	↑	POO	↓	PON	↑
PPO	↑	OON	↓	OPN	↑
NON	↑	OPO	↓	NPO	↑
OPP	↑	NOO	↓	NOP	↑
NNO	↑	OOP	↓	ONP	↑
POP	↑	ONO	↓	PNO	↑

As can be seen in Table 2, the positive and negative redundant small vectors have opposite effects on the neutral point voltage deviation. So, redundant small vectors can be used to achieve neutral point voltage deviation control.

Figure 6 shows the diagram of the proposed control algorithm BLMPVC. The neutral point voltage deviation control strategy adopts hysteresis control. When small vectors are selected in the voltage vector selection process, the predictive deviation of the neutral point voltage predictive deviation U_o^{k+1} at the next moment is predicted by Equation (14). When U_o^{k+1} is no larger than the preset hysteresis width h, neutral point voltage deviation is not carried out, which can reduce the switching frequency further. When the predicted U_o^{k+1} is larger than h, the deviation of U_o is considered to be large. Then, make the inverter output a small vector to reduce the deviation of the neutral point voltage. Although each voltage vector can use a small vector to balance the neutral point voltage deviation, the zero vectors V_0 and V_{26} may make the switch state change between 0 and 2, resulting in a high voltage pulse, which tends to cause the motor winding corrosion and shorten the life of the motor. Therefore, when the inverter outputs zero vectors V_0 and V_{26}, the controller should not implement the neutral point voltage deviation control strategy.
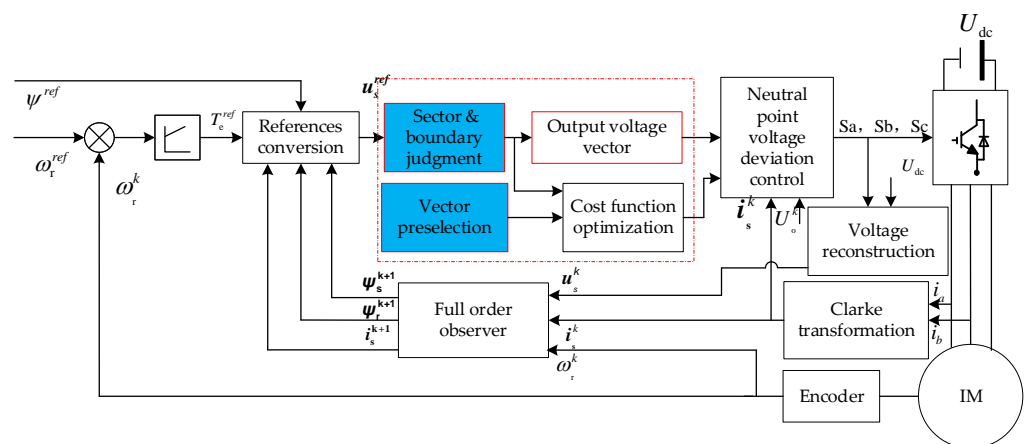

Figure 6. Diagram of BLMPVC.

5. Simulation and Results Discussion

The system simulation model was designed in Matlab/Simulink to verify the effectiveness of the proposed BLMPVC. We investigate the steady state and dynamic performances. To evaluate the performances at lower calculation cost and switching frequency, the state-of-the-art method in [29] is taken as the target of control performance. The parameters in the simulation are shown in Table 3. The sampling frequency of the system is 20 kHz.

Table 3. Parameters of the simulation system.

DC-bus voltage U_{dc}	450 V
Rated power P_N	2.2 kW
Rated voltage U_N	380 V
Rated frequency f_N	50 Hz
Rated torque T_N	14 N·m
Flux amplitude reference ψ^{ref}	0.9 Wb
Number of pole pairs N_p	2
Stator resistance R_s	2.8 Ω
Rotor resistance R_r	2.5 Ω
Mutual inductance L_m	0.212 H
Stator inductance L_s	0.224 H
Rotor inductance L_r	0.224 H
DC-link capacitors C	680 μF
Width of potential hysteresis at neutral point voltage deviation h	5

5.1. Steady State Simulation

In order to analyze the control performance of BLMPVC, the simulation is carried out at rated conditions, i.e., at a given speed of 1500 rpm and a load torque of 14 N·m. To validate the control performance with state-of-the-art, the simulation is also implemented with the method in [29], named MPVC1, in this paper.

As shown in Figure 7, the control performance of BLMPVC can reach the same level as MPVC1, both of which can achieve good control effects. Figure 8 shows the speed comparison between the two methods. Additionally, it can be seen that the speed is almost the same. Figure 9 shows the torque comparison between these two methods. It can be found that the maximum torque ripple of the two methods is about 0.5 N·m, which can meet the overall control requirements well. Further analysis shows that the torque standard deviation of MPVC1 is 0.1648, and the torque standard deviation of BLMPVC is 0.1657 in 2~3 s, which is very close. Figure 10 shows the mean number of voltage vectors enumerated by each control period under no-load and full-load conditions at different speeds with these two control methods. When the motor runs at no load, it can be seen from Figure 10a the enumerating voltage vector of BLMPVC is at most 24.89% of MPVC1 and at least 11.83% of MPVC1 at different speeds. For all the tested speed conditions from 150 rpm to 1500 rpm, the average enumeration vector number of MPVC1 is 9.89, and the average enumeration vector number of BLMPVC is 1.88, which is only 19. 04% of MPVC1. At full load, scenes remain the same. As shown in Figure 10b, the number of voltage vector enumerations with BLMPVC can reduce to 28.66% of that with MPVC1, and even to 17.99% at the speed of 150 rpm, and the average number of enumerations decreases from 9.11 with MPVC1 to 2.07 with BLMPVC, which is only 22.68% of MPVC1. This greatly reduces the calculation cost of the control system and can improve real-time control.
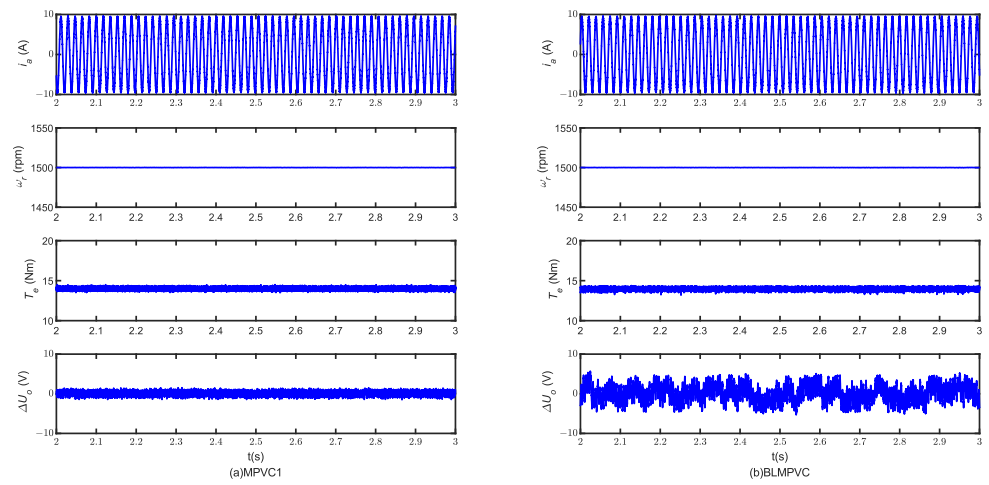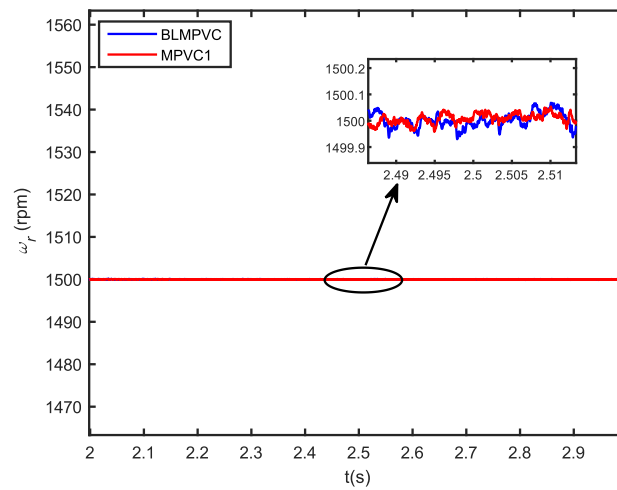
Figure 7. Steadystate performance. (**a**) MPVC1; (**b**) BLMPVC.

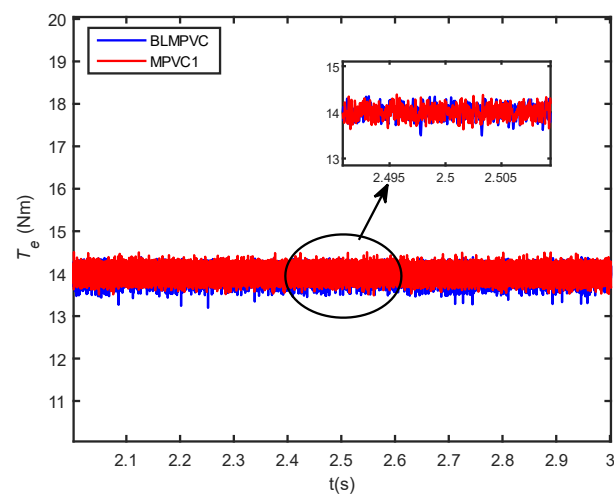**Figure 8.** Steady-state speed responses of MPVC1 and BLMPVC.

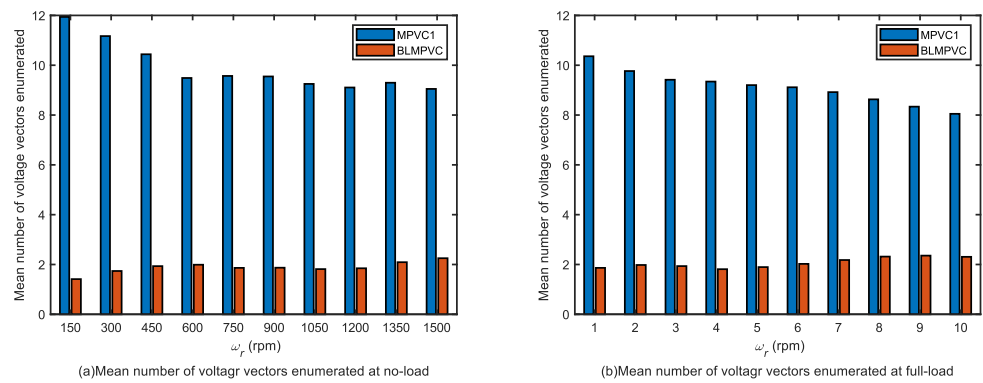**Figure 9.** Steady-state torque responses of MPVC1 and BLMPVC.

(a)Mean number of voltagr vectors enumerated at no-load

(b)Mean number of voltagr vectors enumerated at full-load

Figure 10. Mean number of voltage vectors enumerated. (**a**) no-load; (**b**) full-load.

5.2. Dynamic Simulation

Furthermore, to evaluate the dynamic response performances with disturbances, simulations are carried out at different operation conditions. Additionally, the simulation condition is set as follows. When the motor starts without load, the given speed is 200 rpm, the load torque increases by 10 N·m at 1 s, the given speed changes to 600 rpm at 2 s, the load torque increases by 4 N·m at 3 s, the given speed decreases to 400 rpm at 4 s and accelerates to 1500 rpm at 5 s.

From Figure 11, we can see that the dynamic performances of the two methods are almost the same. Under the condition of the sudden change of given speed and torque, the responses are quick, and the overshoot is in the range of about 3%. The current waveform can also maintain a good sinusoidal degree. Additionally, the neutral point voltage deviation is less than 5 V, which can meet the control requirements. Figure 12 shows the speed responses, and the speed responses of the two methods are almost the same, which means the proposed BLMPVC can gain sound, dynamic performances with fewer switch actions.

Figure 13 shows the comparison between the two control methods' start-up to rated speed with no load, and Figure 14 shows the comparison of the two control methods' start-up to rated speed with full load. It can be seen that the start-up time of both control methods can be maintained at a very high level. The proposed control method BLMPVC can speed up from 0 to 1500 rpm in 0.1 s with no load. Even if the starting speed is slightly reduced at full load, the control system can also start from 0 to 1500 rpm in 0.25 s. In addition, the overshoot of no-load starting is approximately 15 rpm, only at the rate of 1% overshoot, and the overshoot of full-load start is much less, only about 3 rpm.
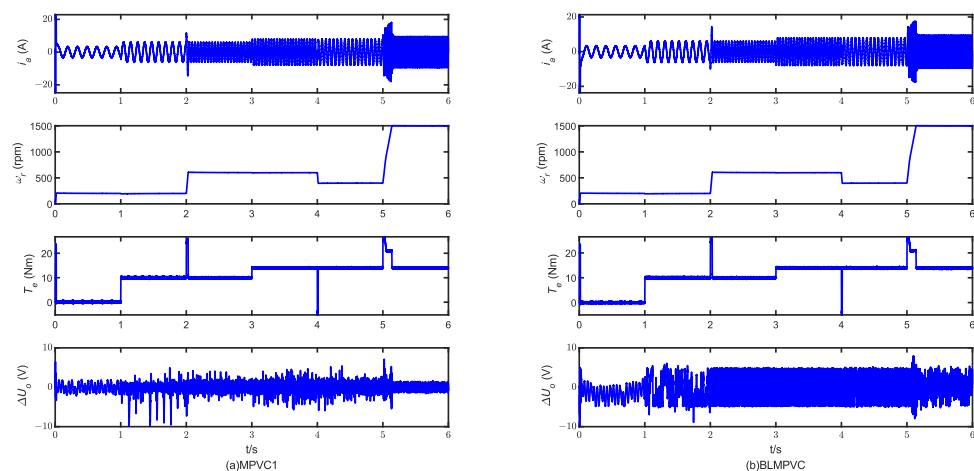

(a)MPVC1

(b)BLMPVC

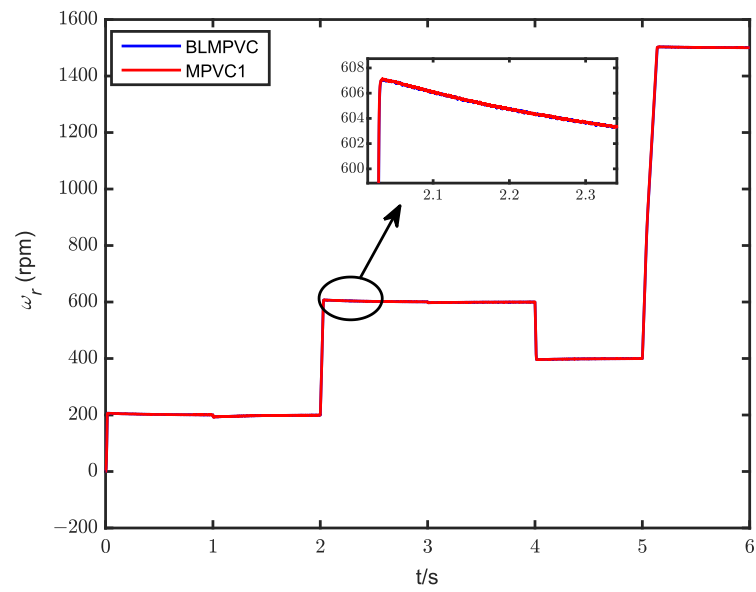**Figure 11.** Dynamic performance comparison. (**a**) MPVC1; (**b**) BLMPVC.

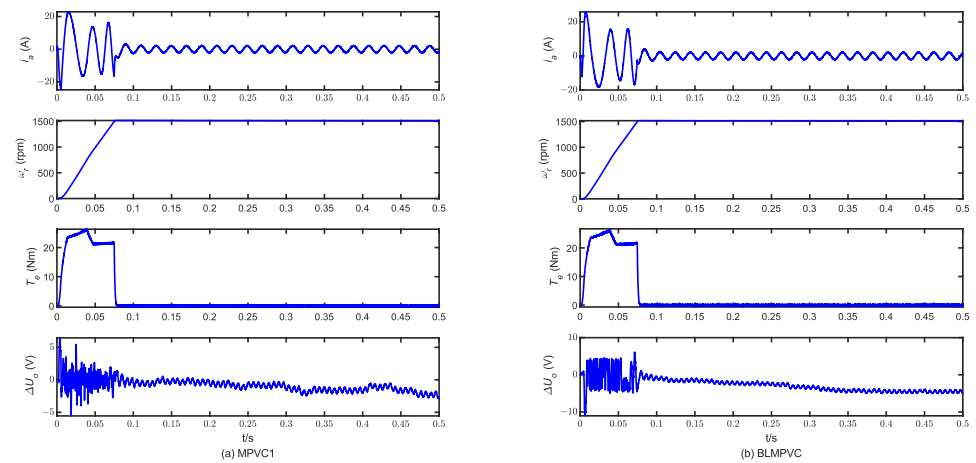**Figure 12.** Dynamic speed responses of MPVC1 and BLMPVC.

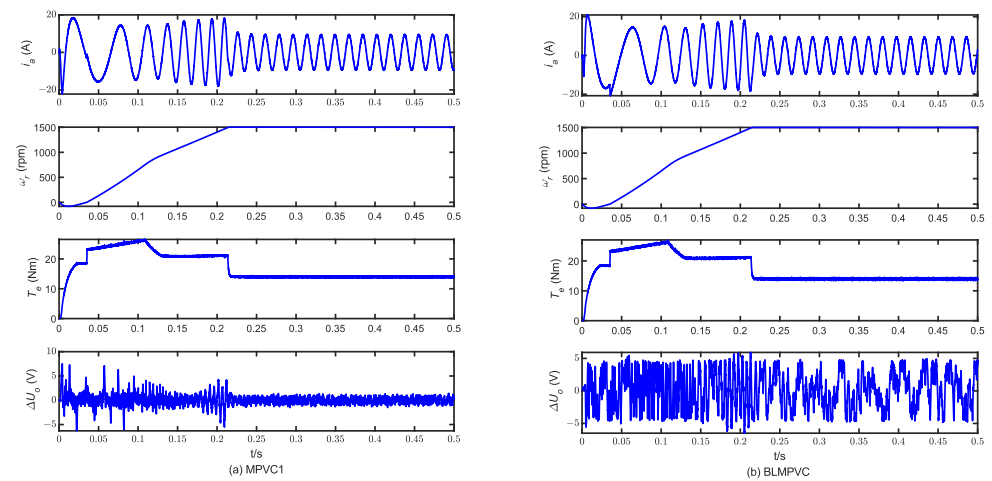**Figure 13.** No-load starting responses of MPVC1 and BLMPVC.

Figure 14. Full-load starting responses of MPVC1 and BLMPVC.

As shown in Figure 15, the number of candidate voltage vectors involved in the enumeration is very different between these two methods. MPVC1 needs to enumerate 5~13 voltage vectors in the control process, but BLMPVC only needs to enumerate 1~3 voltage vectors, which can greatly reduce the calculation amount and improve the real-time performance of the control system.
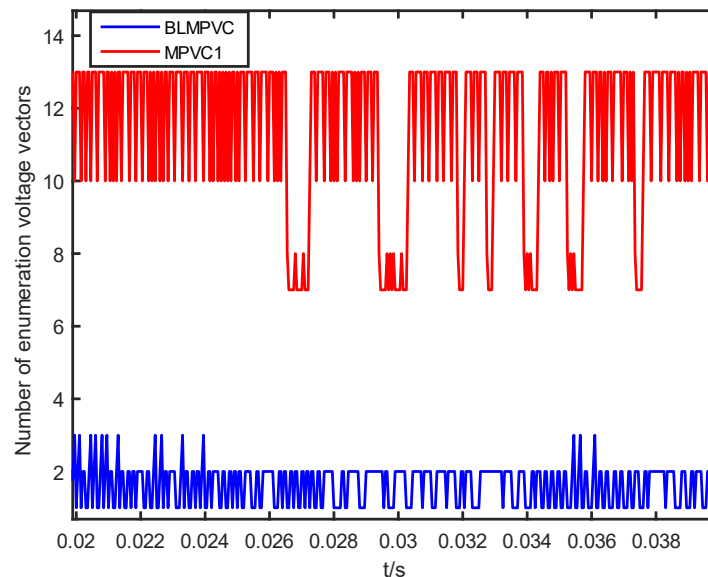

Figure 15. The number change of enumeration voltage vectors of BLMPVC and MPVC1.

5.3. Switching Frequency Analysis

To evaluate the switching frequency reduction in quantity, it is necessary to analyze the actual switch action times. The analysis is based on the simulation with different methods, including traditional MPVC, MPVC1 and BLMPVC.

The average switching frequency can be defined as follows,

$$f_{SW} = \frac{N}{2mzT} \tag{16}$$

where T is the statistical time, N is the total number of switch actions, m is the number of inverter phases, and z is the number of single-phase switching devices. For the 3L-NPC inverter, Equation (16) can be expressed as:

$$f_{SW} = \frac{N}{24T} \tag{17}$$

In this work, Equation (17) is used to calculate the average switching frequency. The results are shown in Tables 4 and 5, which show the average switching frequency at different working states. Table 4 shows the average switching frequency with different methods under no-load conditions, and Table 5 shows the average switching frequency under full-load conditions.

The visual comparison is shown in Figure 16. It can be seen that both MPVC1 and BLMPVC can significantly reduce the switching frequency compared with traditional MPVC. Additionally, in most cases, BLMPVC can significantly reduce the switching frequency compared with MPVC1.

Table 4. The average switching frequency (no-load).

Speed (rpm)	The Average Switching Frequency		
	Traditional MPVC	MPVC1	BLMPVC
150	1367	697	663
300	2147	1130	1100
450	2660	1466	1328
600	2284	1771	1368
750	1845	1572	1151
900	1710	1575	1152
1050	1783	1407	972
1200	1417	1186	931
1350	1708	1102	1034
1500	2111	1110	1171
Mean value	1903	1302	1087

Table 5. The average switching frequency (full-load).

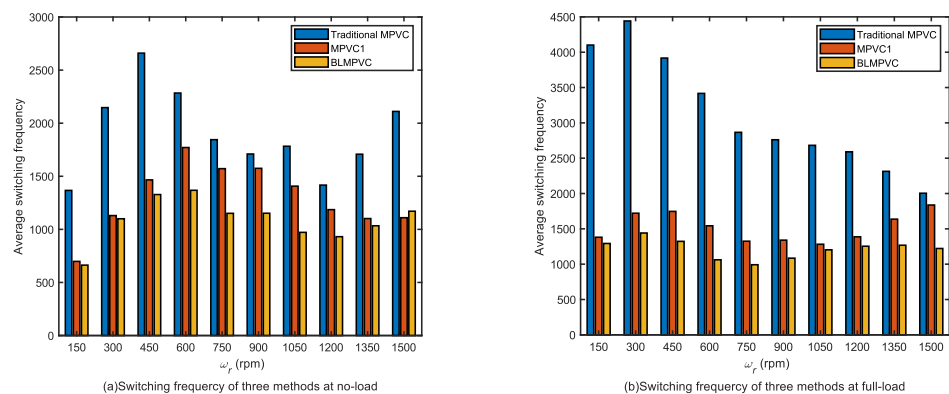| Speed (rpm)	The Average Switching Frequency		
	Traditional MPVC	MPVC1	BLMPVC
150	4101	1381	1293
300	4442	1721	1441
450	3917	1747	1323
600	3417	1543	1062
750	2866	1325	992
900	2761	1340	1085
1050	2682	1282	1203
1200	2590	1387	1254
1350	2314	1637	1268
1500	2004	1837	1222
Mean value	3109	1520	1214

Figure 16. The average switching frequencies. (**a**) no-load. (**b**) full-load.

From Tables 4 and 5, it can be seen that the switching frequency with BLMPVC can be reduced to at least 48.51% compared with traditional MPVC under no-load conditions and to 31.08% under full-load conditions, which can significantly reduce the average switching frequency. Additionally, under no-load conditions, the average switching frequency of MPVC1 is 1302 Hz, while the average switching frequency of BLMPVC is only 1087 Hz, which is reduced by 16.51%. The effect is more significant under full-load conditions; the average switching frequency of MPVC1 is 1520 Hz, while that of BLMPVC is only 1214 Hz, which is reduced by 20.13%. Furthermore, MPVC1 requires 5~13 candidate voltage vectors, and the switching frequency weight coefficient in the cost function needs fine-tuning, while

BLMPVC can effectively reduce the candidate voltage vector and eliminate the weight coefficient in the cost function, which is friendly to the user without complicated weight coefficient tuning.

Through the above analysis, it can be seen that BLMPVC proposed in this paper can achieve excellent control performances while significantly reducing the computation cost and the switching frequency.

6. Conclusions

To achieve sound control performance with low switching frequency for induction motors fed by a 3L-NPC inverter, the BLMPVC control strategy based on vector partition is proposed. By collecting the information on three-phase voltage, three-phase current, and rotation speed, the reference voltage vector at the next time can be predicted using the induction motor model, then the number of candidate voltage vectors is reduced by suitable vector partitioning, and then the calculation cost can be reduced. Furthermore, the switching frequency of the control system is reduced by preselection with boundary circle limitation rules. To balance the neutral point voltage deviation, a strategy with redundant small vectors is carried out. The simulations were implemented on an induction motor fed by a 3L-NPC inverter at no-load and full-load with different control methods. Simulation results show that the proposed method can reduce the switching frequency significantly and also can achieve sound, steady and dynamic characteristics.

References

1. Bazzi, A.M.; Krein, P.T. Review of Methods for Real-Time Loss Minimization in Induction Machines. *IEEE Trans. Ind. Appl.* **2010**, *46*, 2319–2328. [CrossRef]
2. Hannan, M.A.; Ali, J.A.; Mohamed, A.; Hussain, A. Optimization Techniques to Enhance the Performance of Induction Motor Drives: A Review. *Renew. Sustain. Energy Rev.* **2018**, *81*, 1611–1626. [CrossRef]
3. Messaoudi, M.; Flah, A.; Alotaibi, A.A.; Althobaiti, A.; Sbita, L.; Ziad El-Bayeh, C. Diagnosis and Fault Detection of Rotor Bars in Squirrel Cage Induction Motors Using Combined Park's Vector and Extended Park's Vector Approaches. *Electronics* **2022**, *11*, 380. [CrossRef]
4. Varga, T.; Benšić, T.; Jerković Štil, V.; Barukčić, M. Continuous Control Set Predictive Current Control for Induction Machine. *Appl. Sci.* **2021**, *11*, 6230. [CrossRef]
5. Yin, S.; Xia, J.; Zhao, Z.; Zhao, L.; Liu, W.; Diao, L.; Jatskevich, J. Fast Restarting of Free-Running Induction Motors Under Speed-Sensorless Vector Control. *IEEE Trans. Ind. Electron.* **2020**, *67*, 6124–6134. [CrossRef]
6. Aktas, M.; Awaili, K.; Ehsani, M.; Arisoy, A. Direct Torque Control versus Indirect Field-Oriented Control of Induction Motors for Electric Vehicle Applications. *Eng. Sci. Technol. Int. J.* **2020**, *23*, 1134–1143. [CrossRef]
7. Vaez-Zadeh, S.; Jalali, E. Combined Vector Control and Direct Torque Control Method for High Performance Induction Motor Drives. *Energy Convers. Manag.* **2007**, *48*, 3095–3101. [CrossRef]
8. Fu, X.; Li, S. A Novel Neural Network Vector Control Technique for Induction Motor Drive. *IEEE Trans. Energy Convers.* **2015**, *30*, 1428–1437. [CrossRef]
9. Bouguenna, I.F.; Tahour, A.; Kennel, R.; Abdelrahem, M. Multiple-Vector Model Predictive Control with Fuzzy Logic for PMSM Electric Drive Systems. *Energies* **2021**, *14*, 1727. [CrossRef]
10. Zhang, Y.; Yang, H.; Xia, B. Model-Predictive Control of Induction Motor Drives: Torque Control Versus Flux Control. *IEEE Trans. Ind. Appl.* **2016**, *52*, 4050–4060. [CrossRef]
11. Ayala, M.; Doval-Gandoy, J.; Rodas, J.; Gonzalez, O.; Gregor, R.; Rivera, M. A Novel Modulated Model Predictive Control Applied to Six-Phase Induction Motor Drives. *IEEE Trans. Ind. Electron.* **2021**, *68*, 3672–3682. [CrossRef]

12. Zou, J.; Xu, W.; Yu, X.; Liu, Y.; Ye, C. Multistep Model Predictive Control with Current and Voltage Constraints for Linear Induction Machine Based Urban Transportation. *IEEE Trans. Veh. Technol.* **2017**, *66*, 10817–10829. [CrossRef]
13. Ahmed, A.A.; Bakeer, A.; Alhelou, H.H.; Siano, P.; Mossa, M.A. A New Modulated Finite Control Set-Model Predictive Control of Quasi-Z-Source Inverter for PMSM Drives. *Electronics* **2021**, *10*, 2814. [CrossRef]
14. Yan, L.; Dou, M.; Hua, Z.; Zhang, H.; Yang, J. Optimal Duty Cycle Model Predictive Current Control of High-Altitude Ventilator Induction Motor With Extended Minimum Stator Current Operation. *IEEE Trans. Power Electron.* **2018**, *33*, 7240–7251. [CrossRef]
15. Varga, T.; Benšić, T.; Barukčić, M.; Štil, V.J. Optimization of Fuzzy Controller for Predictive Current Control of Induction Machine. *Electronics* **2022**, *11*, 1553. [CrossRef]
16. Norambuena, M.; Rodriguez, J.; Zhang, Z.; Wang, F.; Garcia, C.; Kennel, R. A Very Simple Strategy for High-Quality Performance of AC Machines Using Model Predictive Control. *IEEE Trans. Power Electron.* **2019**, *34*, 794–800. [CrossRef]
17. Xu, W.; Dong, D.; Zou, J.; Liu, Y. Low-Complexity Multistep Model Predictive Current Control for Linear Induction Machines. *IEEE Trans. Power Electron.* **2021**, *36*, 8388–8398. [CrossRef]
18. Yang, Y.; Wen, H.; Fan, M.; Xie, M.; Chen, R. Fast Finite-Switching-State Model Predictive Control Method Without Weighting Factors for T-Type Three-Level Three-Phase Inverters. *IEEE Trans. Ind. Inform.* **2019**, *15*, 1298–1310. [CrossRef]
19. Arahal, M.R.; Satué, M.G.; Barrero, F.; Ortega, M.G. Adaptive Cost Function FCSMPC for 6-Phase IMs. *Energies* **2021**, *14*, 5222. [CrossRef]
20. Wang, S.; Ma, J.; Liu, B.; Jiao, N.; Liu, T.; Wang, Y. Unified SVPWM Algorithm and Optimization for Single-Phase Three-Level NPC Converters. *IEEE Trans. Power Electron.* **2020**, *35*, 7702–7712. [CrossRef]
21. Deng, Y.; Li, J.; Shin, K.H.; Viitanen, T.; Saeedifard, M.; Harley, R.G. Improved Modulation Scheme for Loss Balancing of Three-Level Active NPC Converters. *IEEE Trans. Power Electron.* **2017**, *32*, 2521–2532. [CrossRef]
22. Xiao, D.; Alam, K.S.; Osman, I.; Akter, P.; Rahman, M.F. Low Complexity Model Predictive Flux Control for 3L-NPC Inverter-Fed Induction Motor Drives without Weighting Factor. *IEEE Trans. Ind. Appl.* **2020**, *56*, 6496–6506. [CrossRef]
23. Wang, W.; Zhang, B.; Xie, F. A Novel SVPWM for Three-Level NPC Inverter Based on m-Mode Controllability. *IEEE Trans. Ind. Electron.* **2018**, *65*, 6055–6065.
24. Habibullah, M.; Lu, D.D.-C.; Xiao, D.; Osman, I.; Rahman, M.F. Selected Prediction Vectors Based FS-PTC for 3L-NPC Inverter Fed Motor Drives. *IEEE Trans. Ind. Appl.* **2017**, *53*, 3588–3597. [CrossRef]
25. Xia, Z.; Liu, Z.; Guerrero, J.M. Multi-Objective Optimal Model Predictive Control for Three-Level ANPC Grid-Connected Inverter. *IEEE Access* **2020**, *8*, 59590–59598. [CrossRef]
26. Doan, N.X.; Nguyen, N.V. Improved Model Predictive Control for Asymmetric T-Type NPC 3-Level Inverter. *Electronics* **2021**, *10*, 2244. [CrossRef]
27. Wang, F.; Lin, G.; He, Y. Passivity-Based Model Predictive Control of Three-Level Inverter-Fed Induction Motor. *IEEE Trans. Power Electron.* **2021**, *36*, 1984–1993. [CrossRef]
28. Gao, H.; Zhang, W.; Ren, M.; Liu, X. Three-Level Active Power Filter Based on Model Predictive Control. *Electronics* **2022**, *11*, 1291. [CrossRef]
29. Zhang, Y.; Bai, Y.; Yang, H.; Zhang, B. Low Switching Frequency Model Predictive Control of Three-Level Inverter-Fed IM Drives with Speed-Sensorless and Field-Weakening Operations. *IEEE Trans. Ind. Electron.* **2019**, *66*, 4262–4272. [CrossRef]
30. Zhang, Y.; Yang, H. Two-Vector-Based Model Predictive Torque Control without Weighting Factors for Induction Motor Drives. *IEEE Trans. Power Electron.* **2016**, *31*, 1381–1390. [CrossRef]